

AACVD synthesis and gas sensing properties of nickel oxide nanoparticle decorated tungsten oxide nanowires

Eric Navarrete¹, Carla Bittencourt², Polona Umek³, Eduard Llobet^{*1}

¹MINOS-EMaS, Universitat Rovira i Virgili, Avda. Països Catalans, 26, 43007 Tarragona, Spain

²Chimie des Interactions Plasma – Surface (ChIPS), Research Institute for Materials Science and Engineering, Université de Mons, Avenue Copernic 1, 7000 Mons, Belgium

³Jožef Stefan Institute, Jamova cesta 39, 10000 Ljubljana, Slovenia.

*Correspondence: eduard.llobet@urv.cat; Tel.: +34 977 558 502

Abstract

Here we show that the aerosol assisted chemical vapor deposition process is suitable for growing single crystalline tungsten oxide nanowires loaded with nickel oxide nanoparticles. This method allows for achieving a wide range of nickel oxide loading of tungsten oxide nanowires, with high effectivity. It allows also for the direct growth of these nanomaterials onto application substrates for developing resistive metal oxide gas sensors. Different morphological and compositional analysis tools have been employed for the characterization of the nanomaterials, finding that nickel oxide nanoparticles are homogeneously distributed over the tungsten oxide nanowire surface. However, at high Ni loadings, even though nanoparticles keep their size unchanged, they form agglomerates, especially at the tips of tungsten nanowires. The gas sensing properties of the different nanomaterials grown towards methane, ethanol, nitrogen dioxide and hydrogen sulfide have been studied. The optimized loading of tungsten oxide with nickel oxide nanoparticles has a positive effect for increasing the sensitivity and selectivity of the resulting nanomaterial to hydrogen sulfide, reaching a five-fold increase in the response towards this species. This improvement is attributed to combined chemical and electronic sensitization effects. Therefore, these nanomaterials show good potential for developing inexpensive resistive sensors able to monitor the presence of hydrogen sulfide in the ambient.

Keywords: tungsten oxide, nickel oxide, nanowires, nanoparticles, metal loading, gas sensing.

1. Introduction

The growth in worldwide industrial activity, the ever-growing number of circulating cars and the associated increase in energy demands are boosting global gas emissions ^[1]. This is becoming a serious threat to our environment and to human health ^[2]. As a result, there is a strong demand for developing rugged, sensitive, selective and inexpensive detection systems that could become ubiquitous for reliably monitoring air quality (indoors and outdoors). Resistive metal oxide gas sensors have been the object of sustained research efforts in the last decades, since they meet many of the requirements for integrating inexpensive air-quality monitoring systems ^[3-4]. Highly sensitive to toxic and flammable gases, metal oxides can be mass-produced by employing a wide range of synthesis routes ^[4-5]. Lack of selectivity and cross-sensitivity to ambient moisture remain the most important drawbacks to be overcome.

Most research efforts have been directed towards the study of *n*-type metal oxides such as SnO₂, ZnO, In₂O₃ or WO₃ because these are, generally, more sensitive than *p*-type metal oxides ^[6-9]. The loading of metal oxides with nanoparticles of metal catalysts has been employed extensively both for enhancing sensitivity and tuning selectivity of gas sensors ^[10]. Such nanoparticles can induce chemical sensitization effects. For example, by increasing the amount of reactive oxygen species adsorbed on the surface of the semiconductor metal oxide, and/or by dissociating the target molecules and favoring their reaction with oxygen adsorbates via spillover effects ^[11]. More recently, with the development of single-crystalline, nanostructured metal oxides (e.g. nanorods, nanowires), the synthesis of *n*-type metal oxide nanowires decorated with *p*-type metal oxide nanoparticles has been reported ^[12]. In such a structure, multiple *n*-*p* heterojunctions are formed at the nanoscale, which may lead to important electronic sensitization effects ^[12-13]. Upon the formation of *n*-*p* heterojunctions, electrons are transferred from the *n*-type metal oxide towards the *p*-type nanoparticles and depletion zones develop. When gaseous species adsorb onto nanoparticles, this results in additional electronic charge transfer between the *p*-type nanoparticles and the supporting *n*-type metal oxide, modifying the width of depletion zones and dramatically altering the overall electrical conductance of a film. Recently, we have developed two examples of such an approach. In the first case, films of single-crystalline, *n*-type tungsten oxide nanowires decorated with *p*-type copper oxide were devised for the selective detection of hydrogen sulfide.

When in the presence of H₂S, p-type copper oxide becomes metallic copper sulfur by a mechanism of oxygen-sulfur replacement. While p-n heterojunctions are destroyed, a high number of electrons is released towards the n-type metal oxide nanowires and the conductivity of the film is highly increased [14]. In a second example, n-type tungsten oxide nanowires decorated with p-type palladium oxide were employed for the selective detection of hydrogen. In this case, similarly to the previously described situation, p-type palladium oxide becomes metallic palladium hydride in the presence of hydrogen at low operating temperatures [15]. These sensors are reversible because copper sulfide and palladium hydride become again copper or palladium oxides when hydrogen sulfide or hydrogen are removed from the sensor environment, respectively [14,15].

Late transition metals such as the already mentioned copper and palladium or platinum [16], oxidize to p-type metal oxides due to normal operation during gas sensing. In that sense, it is worth exploring the loading of n-type metal oxides with other p-type, late transition metal oxide nanoparticles and study the implications in sensitivity and selectivity. This paper addresses the loading of tungsten oxide nanowires with nickel oxide nanoparticles (NiO). NiO has been known to be p-type metal oxide for a long time, with a reported large work function of 5.4 eV and optical bandgap ranging from 3.6 to 4.0 eV [17]. Its p-type character is attributed to the spontaneously formed Ni vacancies [18]. The use of NiO for gas sensing has been reported already. For example, Kim and co-workers [19] and Yoon and co-workers [20] employed Fe-doped, p-type NiO for detecting 100 ppm of ethanol. Cho and co-workers reported Pt-doped, p-type NiO nanotubes for detecting ethanol [21]. Huo and co-workers reported the high response of NiO nanowall arrays to hydrogen sulfide [22]. Additionally, loading p-type NiO nanoparticles onto n-type metal oxide structures has been shown to increase gas sensing performance (e.g., by lowering response times or humidity cross-sensitivity) [23]. NiO supported by ZnO structures has been reported for detecting ammonia [24] and nitrogen dioxide [25]. NiO combined to indium oxide [26] or NiO supported onto tin oxide nanofibers [27] have been studied for detecting ammonia and nitrogen dioxide, respectively. Nickel oxide supported by thin or thick tungsten oxide films has been reported as well. Noh and co-workers employed a sol-gel method to incorporate NiO into a tungsten oxide matrix for developing a nitrogen dioxide sensor [28]. Vuong and co-workers loaded a sputtering-deposited tungsten oxide thin film with Ni₂O₃ [29]. They grew by arc-discharge carbon nanotubes on top of the tungsten oxide film employing Ni as catalyst, which was followed by a

calcination process to burn out carbon nanotubes, leaving nickel oxide nanoparticles. These films were applied to the detection of ammonia vapors. One of the problems associated to the use of high temperatures during calcination steps is the formation of NiWO₄ species, which act as a charge barrier, decreasing sensor performance.

Here we report the growth and gas sensing properties of NiO nanoparticles supported by tungsten oxide nanowires. An aerosol assisted chemical vapor deposition method (AACVD) is used, which is run at temperatures that avoid the formation of NiWO₄. This paper presents an in-depth characterization of the morphology and chemical composition of the nanomaterials synthesized, and addresses the effects of NiO loading in their gas sensing properties. It explores selectivity, cross-sensitivity to ambient moisture and discusses gas sensing mechanisms. To the best of our knowledge, the loading of tungsten oxide nanowires with nickel oxide nanoparticles for gas sensing has been reported only once before. This was a conference paper in which we presented very preliminary, incomplete results ^[30].

2. Experimental

2.1. Material synthesis

Pure and Ni-decorated forests of tungsten oxide nanowires were grown by aerosol assisted chemical vapor deposition (AACVD). Tungsten hexacarbonyl (W(CO)₆) 97% purity and nickel(II) acetylacetonate (Ni(acac)₂) 95% purity, both from Sigma-Aldrich were used without further purification for obtaining tungsten oxide and nickel oxide nanoparticles, respectively. Two approaches, i.e. single-step or two-step growth, were considered for the synthesis of nanomaterials. At first, a single step growth was implemented. In this strategy W(CO)₆ and Ni(acac)₂ are dissolved in an mixture of acetone and methanol and the AACVD process is run to obtain Ni-decorated tungsten oxide nanowires. Despite our efforts for optimizing the acetone/methanol ratio and deposition temperature (these two parameters have a strong influence in the morphology of the resulting nanomaterials), this one-step approach failed to produce homogeneously decorated tungsten oxide nanowires with a wide enough range of Ni loading (see the Supporting Information). In the second approach, at first pure tungsten oxide nanowires are grown by AACVD. Then, a second AACVD process is conducted to decorate some of the previously grown tungsten oxide nanowire samples with nickel oxide

nanoparticles. Employing this two-step approach, samples of tungsten oxide nanowires with four different levels of Ni loading were obtained.

When growing pure tungsten oxide nanowires, the precursor solution was prepared by dissolving 50 mg of tungsten hexacarbonyl in an acetone:methanol (ratio 3:1) mixture. This solution was placed under ultra-sonication to form an aerosol, which was input to the reactor chamber using a 0.5 L/min nitrogen flow. The reactor was kept at 400 °C during the whole deposition process, which lasted until the total consumption of the precursor solution. The deposition took place, via a shadow mask, onto the electrode area ($2.5 \times 2.5 \text{ mm}^2$) of commercially available alumina transducers (Ceram Tech GmbH, Plochingen, Germany). Transducers consist of a pair of Pt interdigitate electrodes (front side) with an electrode gap of 300 μm , and a Pt heating resistor (back side). As-deposited tungsten oxide nanowire films display a dark-blue color, which is due to tungsten oxide being sub-stoichiometric and to carbon residues from the precursors and solvents used. Coated transducers were then placed inside a muffle to undergo an annealing treatment at 500 °C under a flow of pure dry air. Annealed samples display a pale-yellow color indicating that most of carbon contamination has been removed and tungsten oxide is close to stoichiometric. For those samples in which tungsten oxide was loaded with different amounts of Ni, a second AACVD process was conducted. For achieving 4 different levels of Ni loading, in this second step four methanol solutions having different Ni(acac)₂ concentrations were used (i.e., 2.5, 5, 10 and 15 mg of nickel precursor dissolved in 10 mL of methanol). Nitrogen flow and deposition temperature were identical to the ones employed during the first step. A second annealing process was performed as well employing the same conditions described above.

The crystalline phase, morphology and chemical composition of the different nanomaterials grown on transducer substrates were investigated employing X-ray diffraction (XRD), scanning electron microscopy (SEM), high-resolution transmission microscopy (HR-TEM), energy-dispersive X-ray spectroscopy (EDX) and X-ray photoelectron spectroscopy (XPS). XRD was performed employing a Bruker-AXS D8-Discover diffractometer with a parallel incident beam. Scanning electron microscopy images were acquired using a SU8020 Microscope from Hitachi and a JEOL 7600F field emission SEM. The image resolution was set to 512×384 pixels while the corresponding map resolution was set to 128×96 pixels, meaning a pixel size of 0.01 μm in the image and of 0.05 μm in the map. EDX spectra were acquired using a microanalysis tool from

Oxford Instruments. HRTEM characterization of the samples was performed on a Jeol 2100 microscope, working at 200 kV. XPS was conducted using a VERSAPROBE PHI 5000 from Physical Electronics, equipped with a monochromatic Al K α X-ray source. The X-ray photoelectron spectra were collected at the take-off angle of 45° with respect to the electron energy analyzer operated in the CAE (constant analyzer energy) mode. For the compensation of built-up charge on the sample surface during the measurements, a dual beam charge neutralization composed of an electron gun (≈ 1 eV) and an Ar ion gun (≤ 10 eV) was used. Binding energies are all referred to the C1s peak at 284.6 eV.

2.2. Gas sensing experiments

The gas sensing properties of the different nanomaterials were investigated. In particular, the main objective was to study how different levels of Ni loading affected the gas sensing properties of tungsten oxide nanowires. For doing so, AACVD-grown, pure tungsten oxide and Ni-loaded tungsten oxide nanowire sensors were placed inside an inert, airtight Teflon[®] chamber. Calibrated gas bottles of ethanol, methane, hydrogen sulfide and nitrogen dioxide balanced in air were employed. The carrier gas was zero-grade dry air. A computer-driven, automated mass-flow control system was employed to deliver reproducible concentrations of the different gases and vapors tested to the sensor chamber. The concentrations measured were 5, 10, 15 and 20 ppm for ethanol and methane; 10, 15, 25 and 50 ppm for hydrogen sulfide and 10 ppm for nitrogen dioxide. The baseline of sensors was recovered under dry air. A 100 mL/min constant flow was input to the gas sensor chamber. During experiments, the dc electrical resistance of the sensors was monitored, acquired and stored employing a Keysight 3972A data acquisition system. The heating resistors of the sensors were driven by an Agilent U8001A power supply to set the operating temperature. Operating temperatures were set at 150, 200 and 250 °C. Achieving good sensing performance at low-moderate operating temperatures is essential to reduce power consumption. A liquid mass flow was employed as well in some specific measurements to humidify the gas flow and analyze the effect of moisture cross-sensitivity.

3. Results and discussion

3.1. Initial assessment of gas sensing properties

An initial screening of gas sensing properties was conducted to determine whether it was worth studying in depth all four levels of Ni loading. The responses to different concentrations of hydrogen sulfide, ethanol and nitrogen dioxide were measured for pristine, and the Ni-loaded samples. Sensor response was defined as $R_{\text{air}}/R_{\text{gas}}$ for reducing species and $R_{\text{gas}}/R_{\text{air}}$ for oxidizing species, where R_{air} is the resistance of the sensor in pure air (i.e., baseline resistance) and R_{gas} is the resistance of the sensor exposed to a given gas or vapor. Figure 1 shows the dynamic response and recovery for the different nanomaterials and species tested. For easing the comparison, the responses of each sensor appear normalized (i.e. for each sensor the instantaneous resistance is divided by its initial baseline resistance value). Two main conclusions can be derived from these results. Some levels of Ni loading result in higher responses to the different species tested than those observed for pristine tungsten oxide. The higher levels of Ni loading, i.e., those achieved employing 10 and 15 mg of nickel precursor during the AACVD process, resulted in decreased responsiveness. In metal oxide gas sensors, it is well known that too high a level of metal loading results in decreased responsiveness [5].

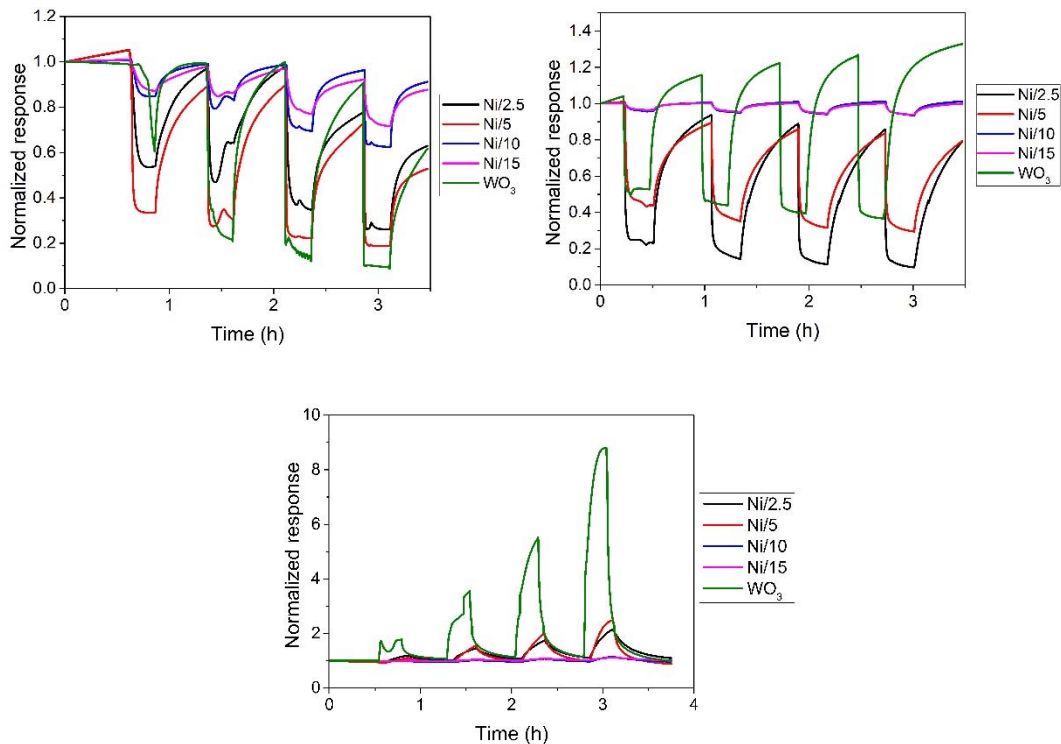


Figure 1. Normalized dynamic response and recovery cycles of sensors that correspond to the full range of Ni loading levels. Sensors were operated at 200 °C. The different panels correspond to H₂S (upper left), ethanol (upper right) and NO₂ (lower).

Considering these results, from now on the high levels of Ni loading are no further studied. Only samples consisting of pure tungsten oxide and Ni loaded samples obtained employing 2.5 and 5 mg of nickel precursor are discussed. These samples are labelled as WO_3 , Ni/LC and Ni/HC, respectively.

3.2. Material characterization

An XRD study was performed to obtain the crystallographic structure of pure and Ni-loaded WO_3 nanowires. No reflection peaks due to the presence of Ni were observed in Ni/LC nor Ni/HC samples. This is generally the case in AACDV grown, metal loaded tungsten oxide nanowires^[14-16]. These results are summarized in Figure 2. The diffraction pattern of the pure WO_3 nanowire sample correspond to monoclinic structure of WO_3 (space group $P_{2/m}$, JPCDS 73-2177), while diffraction patterns of both Ni-loaded samples (Ni/LC and Ni/HC) correspond to triclinic structure of WO_3 (space group $P-1$, JPCDS 73-0305). These differences are attributed to the fact that pure tungsten oxide samples undergo only one annealing step after the AACVD growth. In contrast, Ni-loaded samples undergo a second annealing step, which is run after the second AACVD process used to load pure tungsten oxide with Ni.

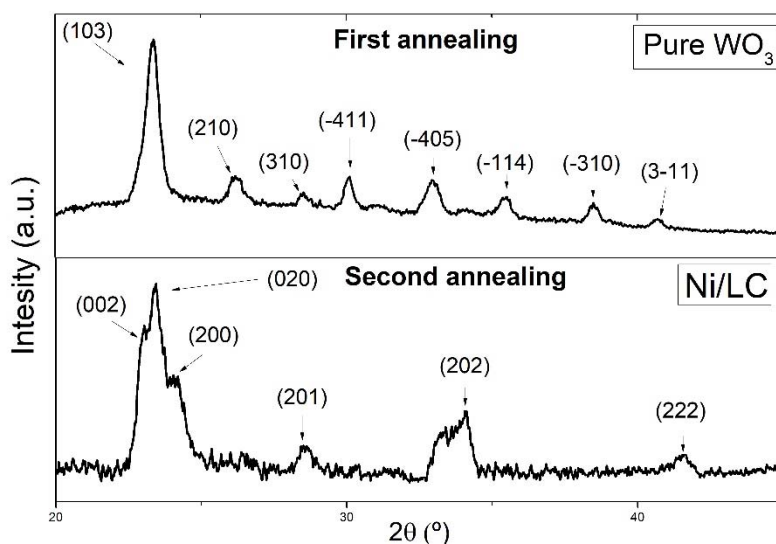


Figure 2. Typical XRD spectra recorded on a pure tungsten oxide nanowire film, $\text{W}_{2.72}\text{P}2/m$ (upper panel) and Ni-loaded tungsten oxide nanowire film, WO_3 $P-1$ (lower panel) (Ni/LC). Pure tungsten oxide samples have undergone one annealing step only and show a monoclinic structure. Ni-loaded tungsten oxide samples have undergone two annealing steps and show a triclinic structure.

Figure 3 shows SEM micrographs for pure (Fig. 3 left panel) and for Ni-loaded (Fig. 3 right panel) tungsten oxide films. Both films show a similar morphology consisting of a carpet of randomly oriented nanowires. The length of nanowires typically ranges between 4 and 12 μm and their diameter ranges from 60 to 150 nm. Some dendritic, flower-like structures are visible for both pure and Ni-loaded samples in the higher magnification insets in Figure 3. These structures are more apparent in Ni-loaded samples. Figure 4 shows a higher magnification SEM micrograph taken from a Ni-loaded sample (Ni/HC). This micrograph shows that tungsten oxide nanowires are decorated with small nanoparticles. At the tip of nanowires, these particles form bigger agglomerates in broccoli-shaped structures. EDX (see the Supporting Information) confirms the presence of Ni in Ni-loaded samples.

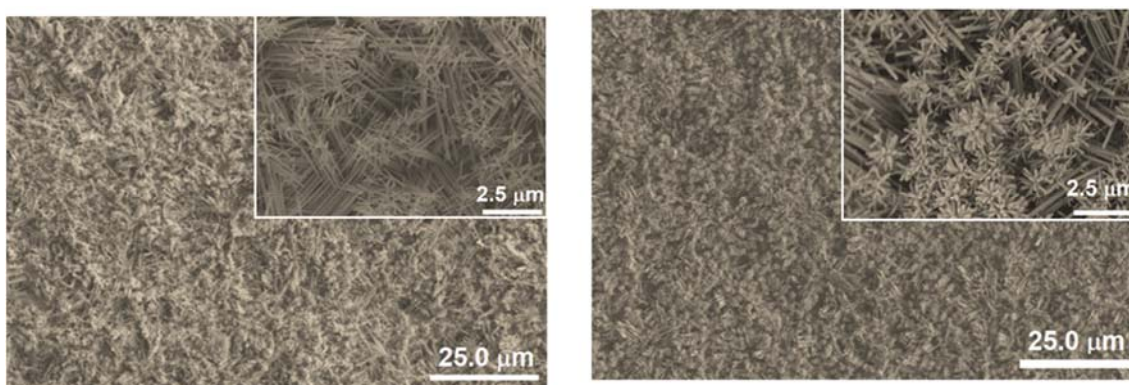


Figure 3. Typical ESEM micrographs for pure tungsten oxide nanowire films (left panel) and, for Ni-loaded tungsten oxide nanowire films (right panel) (Ni/HC). The insets show that flower-like nanostructures appear in both type of samples, however these are more visible in Ni-loaded samples. Ni loaded tungsten oxide nanowires were grown employing the two-step AACVD procedure.

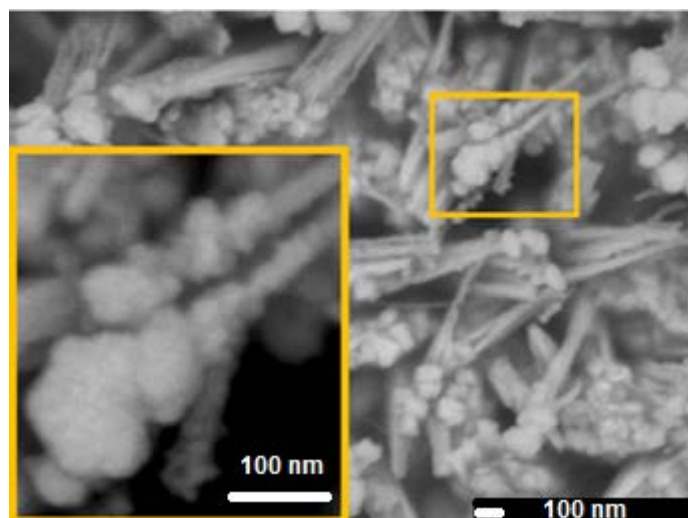


Figure 4. SEM micrograph of the Ni/HC sample. A micrograph was taken at higher magnification for an area previously shown in the right panel of Figure 3. Few-nanometer sized nanoparticles appear decorating the surface of tungsten oxide nanowires. Bigger agglomerates of such nanoparticles appear at the tips of nanowires (see the inset).

SEM and TEM micrographs of the Ni/LC sample shown in Figure 5 reveal that tips of WO_3 nanowires are covered with particles. Similar results were observed for the Ni/HC sample (Figure 4), however, the size of particles and their amount is significantly lower than in the case of the Ni/HC sample. This agrees well with the fact that for the coverage of WO_3 nanowires for the Ni/LC sample a lower concentration of the nickel precursor was used. From the inset in TEM micrograph is evident that particles observed at the surface are actually agglomerates composed of nanoparticles with diameters up to 2 nm. Nanoparticles appear to be amorphous and therefore the presence of Ni was only proved with EDX analysis (see Supporting information) and their chemical nature with the XPS (results are discussed later). In addition, WO_3 nanowires in both Ni-loaded samples are crystalline (see supporting information); clear lattice fringes of 0.39 nm are observed corresponding to the interplanar spacing of (002) planes in WO_3 with triclinic structure (JPCDS 71-0305) thus agreeing with the results of XRD analysis (Figure 2).

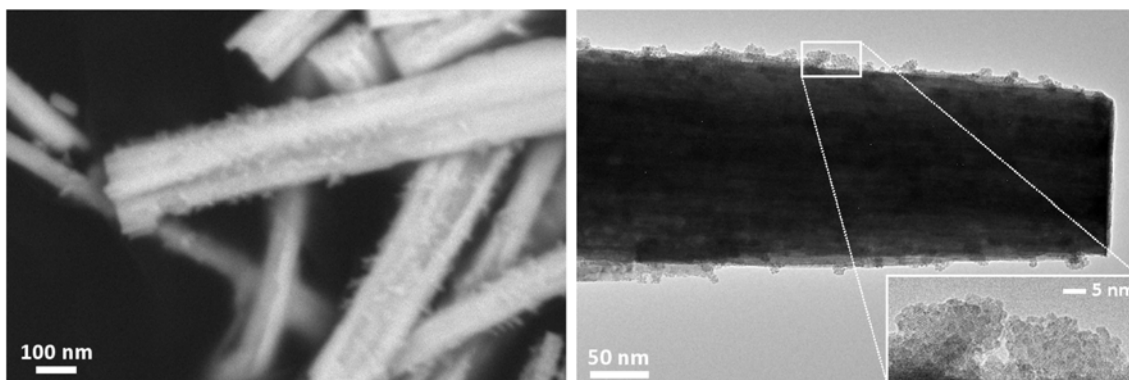


Figure 5. SEM (left) and TEM (right) micrographs obtained from the Ni/LC sample. The inset in the TEM image is an enlargement of the area indicated.

XPS was used for elemental and chemical analysis of the Ni-loaded, nanostructured active layers. Figure 6.a shows the typical survey spectrum recorded on the Ni doped samples in the range 0–950 eV binding energy. In addition to the expected characteristic peaks related to the photoelectrons emitted from tungsten and oxygen atoms, we can

observe the presence of peaks related to the presence of nickel and carbon. The adventitious carbon contamination due to exposure to atmosphere is used as a charge reference, C-C peak at 284.6 eV. Figure 6.b shows the W 4f XP spectrum recorded on a Ni/HC sample and its fitting analysis, the spectrum was fitted using two doublets, a singlet and the Shirley background. The components centered at 41.2 eV, 37.6 and 35.5 eV are generated by photoelectrons emitted from the W 5p_{3/2}, W 4f_{5/2} and W 4f_{7/2} core level states, respectively in stoichiometric WO₃ (oxidation state +6)^[31]. In stoichiometric WO₃, the W ions have their 5d shell empty, i.e., there are no cation d-electrons available to be transferred to adsorbates. The second W 4f doublet, at 36.4 eV and 34.1 eV corresponding to W 4f_{5/2} and W 4f_{7/2} core level states, was associated with photoelectrons emitted from tungsten atoms near oxygen vacancies VO^[32]. In this case, the d-electron orbitals on adjacent cations are partially occupied. These reduced cations provide active sites for chemisorption and catalytic activity, i.e., influencing gas-sensing activity of the films^[33]. From the area ratio of the components used to fit the W 4f peak we evaluated that near 3.5% of the tungsten atoms are near oxygen vacancies, thus contributing to gas detection.

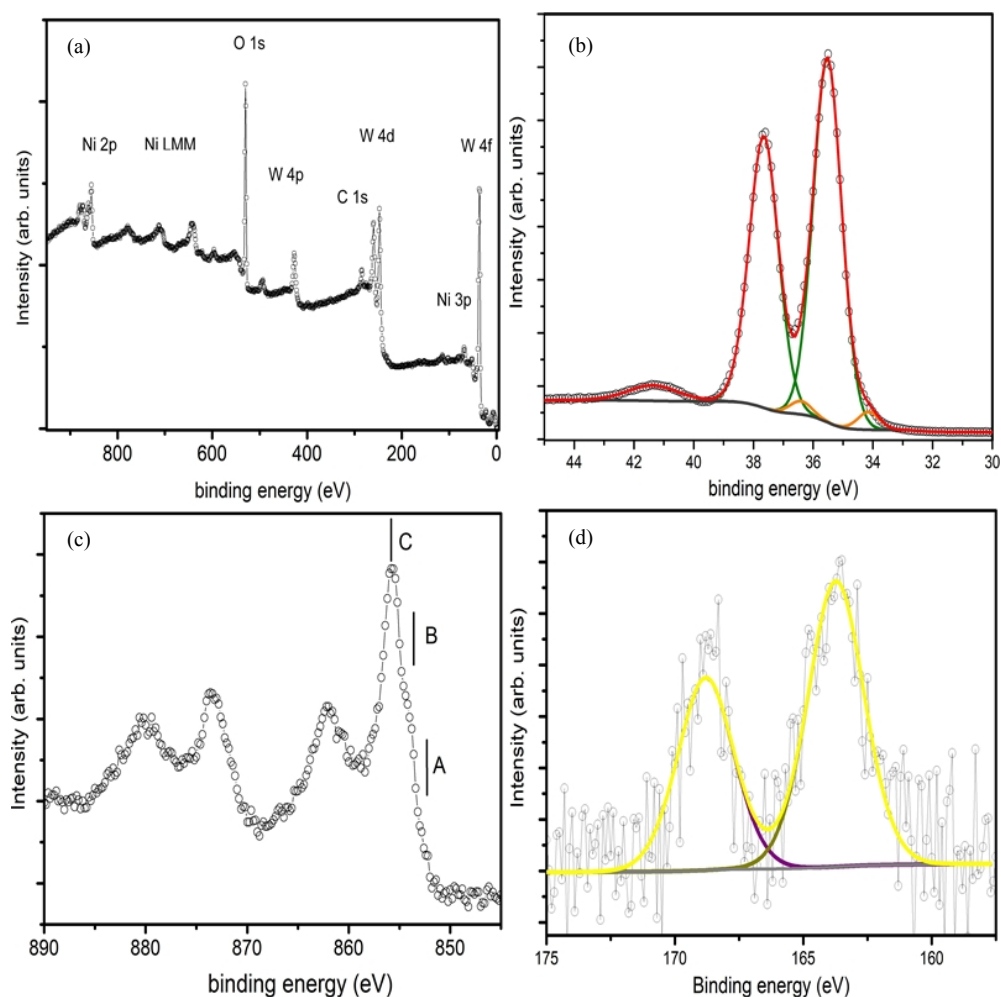


Figure 6. a) XPS spectrum of WO₃:Ni/HC; b) W 4F XPS spectra sample WO₃:Ni/HC; c) Ni 2P XPS spectrum (WO₃:Ni/HC); d) Fitting of sulfur peaks showing Ni-S in the form of Ni_xS_x and Ni_xS_xO_x.

In order to increase the sensing activity of the WO₃ Ni atoms were added. Inspecting the typical XPS spectrum recorded before sensing we observe the presence of peaks that can be associated to photoelectrons emitted from Ni, W, carbon and oxygen atoms (figure 6.a). The relative concentration of elements is shown in Table 1. The low intensity component in the 4f W peak suggests that the WO₃ is slightly reduced (figure 6.b). The XPS spectrum of Ni 2p_{3/2} peak clearly demonstrates that the NiO (Ni²⁺, 854.7 eV), Ni₂O₃ (Ni³⁺, 855.8 eV) and metallic (Ni⁰, 853.1 eV) phases coexist. After sensing we observed the presence of sulfur atoms at the sample surface, the XPS sulfur spectra recorded on the samples testify the formation of Ni-S in the form of Ni_xS_x and Ni_xS_xO_x.

Table 1. Sensing layer average composition in atomic percentage (atom. %) before gas exposure, as obtained from the XPS analysis

	W	O	Ni
Ni/LC	17.5	72.0	10.5
Ni/HC	20.0	65.0	15.0
WO ₃	25.0	75.0	0

3.3. Gas sensing properties

The sensors were tested to several concentrations of methane, ethanol, nitrogen dioxide and hydrogen sulfide balanced in pure dry air. Three different operating temperatures were considered, i.e. 150 °C, 200 °C and 250 °C. Lower operating temperatures were not considered because these often resulted in increased response times. Higher operating temperatures were not considered either, because this significantly increases power consumption.

3.3.1. Methane results

The sensors were tested under a flow of methane at concentrations that ranged from 5 to 20 ppm. The response towards methane of tungsten oxide based sensors was small. When

operated at 150 °C, sensors showed no response to methane. Methane response slightly increased with operating temperature. Figure 7 summarizes these results. It was necessary to operate the sensors at 250 °C to obtain reliable results. Pure tungsten oxide shows very small response to methane. Loading with Ni results in a slightly increased response and the lower level of Ni loading results in the highest response enhancement towards methane.

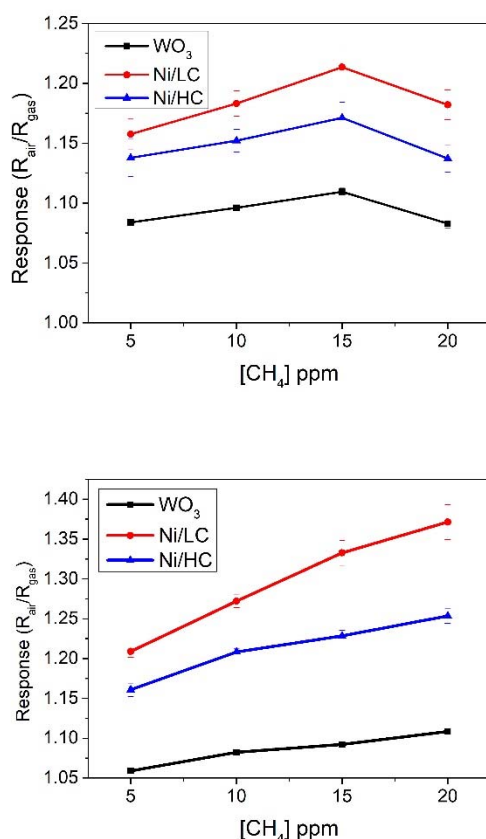


Figure 7. CH₄ detection results for the different sensors operated at 200 °C (upper panel) and 250 °C (lower panel). When operated at 150 °C (not shown), sensors showed no response towards methane.

3.3.2. Ethanol results

Sensors were exposed to ethanol vapors at concentrations of 5, 10, 15 and 20 ppm balanced in dry air. The results of ethanol detection are summarized in Figure 8. When sensors are operated at 150 °C, pure tungsten oxide shows better ethanol responsiveness than Ni-loaded tungsten oxide. In contrast, when the operating temperature is raised, Ni-loaded tungsten oxide samples show higher responsiveness to ethanol vapors than pure

tungsten oxide. In this case the higher Ni loading level results in the highest increase in response. However, ethanol sensitivity, i.e. the slope of the curves shown in Figure 8, is very similar for pure tungsten oxide operated at 150 °C (best sensitivity for pure WO₃) and for Ni-loaded tungsten oxide operated at 250 °C (best sensitivity for Ni-loaded WO₃). It can be concluded, therefore, that Ni loading is not clearly advantageous for increasing ethanol sensitivity.

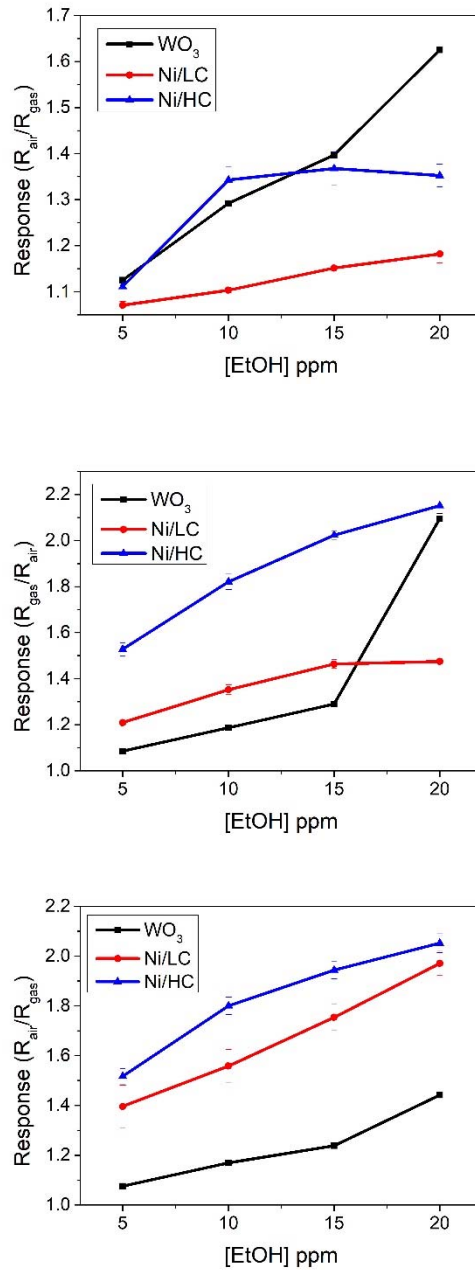


Figure 8. Ethanol detection results for the different sensors operated at 150 °C (upper panel), 200 °C (middle panel) and 250 °C (lower panel).

3.3.3. Nitrogen dioxide results

In order to analyze the response of the different materials towards oxidizing species, the response towards NO_2 was studied. In this case, a single concentration of 10 ppm was measured at the three different operating temperatures. Results are shown in Figure 9. The loading of tungsten oxide with Ni results in increased nitrogen dioxide responsiveness. For both pure WO_3 and Ni-loaded tungsten oxide (lower Ni concentration) the best response was obtained at the lower operating temperature. In the case of Ni-loaded tungsten oxide (higher Ni concentration), 200 °C was the best operating temperature for detecting nitrogen dioxide. In fact, highly loaded Ni- WO_3 operated at 200 °C resulted in the highest response value for NO_2 .

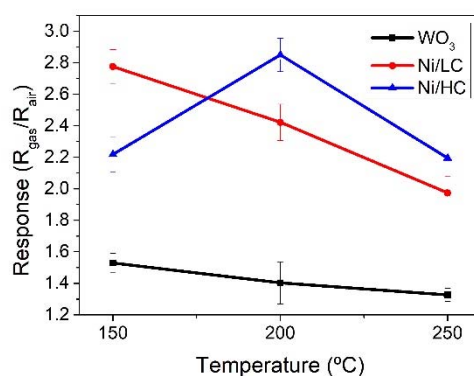


Figure 9. NO_2 sensing results for the different materials studied as a function of the sensor operating temperature.

3.3.4. Hydrogen sulfide results

The responses towards different concentrations of hydrogen sulfide that ranged between 10 and 50 ppm in a balance of pure dry air were measured. When operated at 150 °C the loading of the sensing layer with Ni has negative effects on sensor response, because lower responses towards hydrogen sulfide are recorded for Ni-loaded tungsten oxide than for pure WO_3 samples. As the operating temperature increases this behavior is gradually reversed and the response towards hydrogen sulfide is significantly increased for Ni-loaded samples in comparison to pure tungsten oxide. Highly loaded Ni- WO_3 samples show the highest responsiveness towards hydrogen sulfide when operated at 250 °C with the Ni/HC sensor. A 5-fold increase in responsiveness is obtained. These results are summarized in Figure 10.

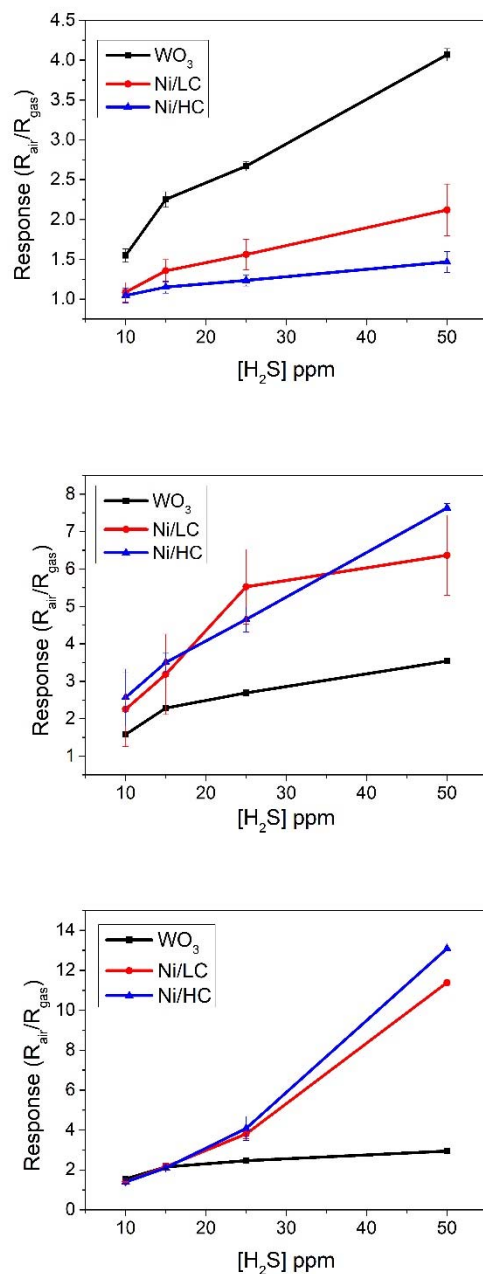


Figure 10. Hydrogen sulfide detection results for the different sensors operated at 150 °C (upper panel), 200 °C (middle panel) and 250 °C (lower panel).

In the detection of hydrogen sulfide, the loading of tungsten oxide nanowires with nickel oxide nanoparticles is clearly beneficial, since it significantly increases response. This is summarized in Figure 11, which supports that the nickel oxide loading of tungsten oxide enhances response and selectivity towards hydrogen sulfide. In addition, the response time of this sensor to hydrogen sulfide is about 88 s, which compares favorably to its response times to the other species tested (further details can be found in the Supporting Information).

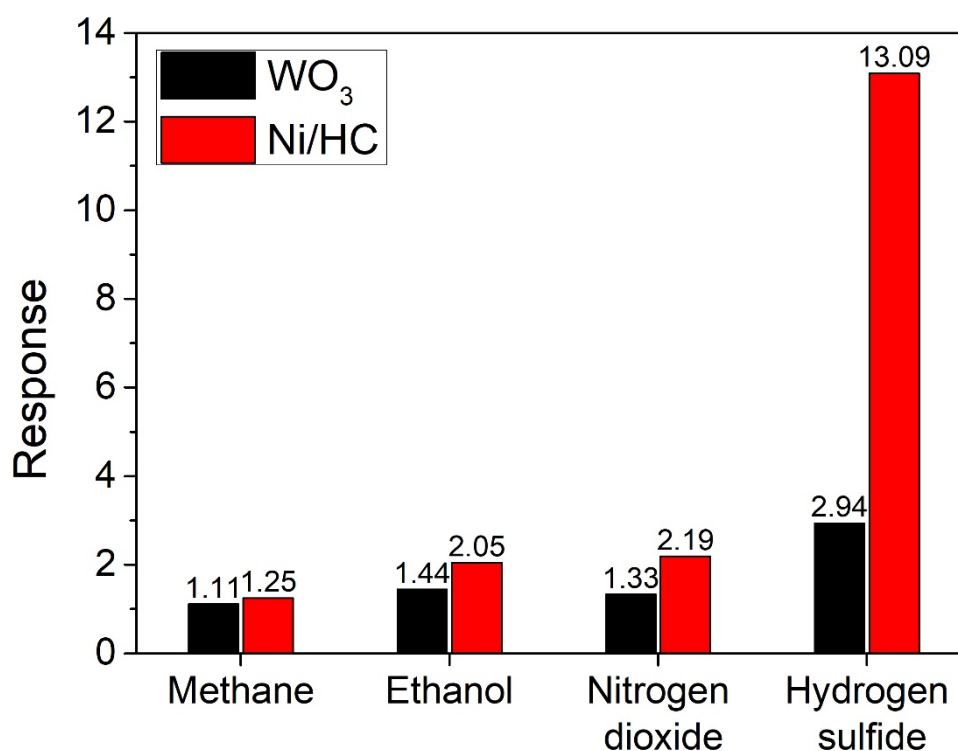


Figure 11. Comparison of response intensities ($R_{\text{air}}/R_{\text{gas}}$ for reducing gases and $R_{\text{gas}}/R_{\text{air}}$ for oxidizing gases) for a pure WO_3 sensor and a Ni/HC WO_3 sensor both operated at 250 °C.

3.3.5. Effect of ambient humidity on the response towards hydrogen sulfide

So far, the analysis of the gas sensing properties has been conducted under dry conditions. However, to better simulate the normal working conditions of the sensors in a real application the effect of ambient humidity needs to be considered as well. Therefore, hydrogen sulfide diluted in humid air was measured in order to study humidity cross-sensitivity in Ni-loaded tungsten oxide nanowire sensors. The results obtained (see Figure 12) show that the presence of ambient moisture increases the intensity of sensor response for low hydrogen sulfide concentrations (i.e. ≤ 25 ppm). However, at higher hydrogen sulfide concentrations (e.g. 50 ppm) the response decreases in the presence of moisture. This response saturation results in a loss of sensitivity. However, in a real application hydrogen sulfide should be measured in the units of ppm range rather than in the tens of ppm range. For example, the Association Advancing Occupational and Environmental Health recommends a threshold limit value (TLV) of 1 ppm as an 8-hour time weighted average (TWA) and a short-term exposure limit (STEL) of 5 ppm for hydrogen sulfide ^[34]. These concentrations would be easily detectable by the Ni-loaded sensor under humid conditions.

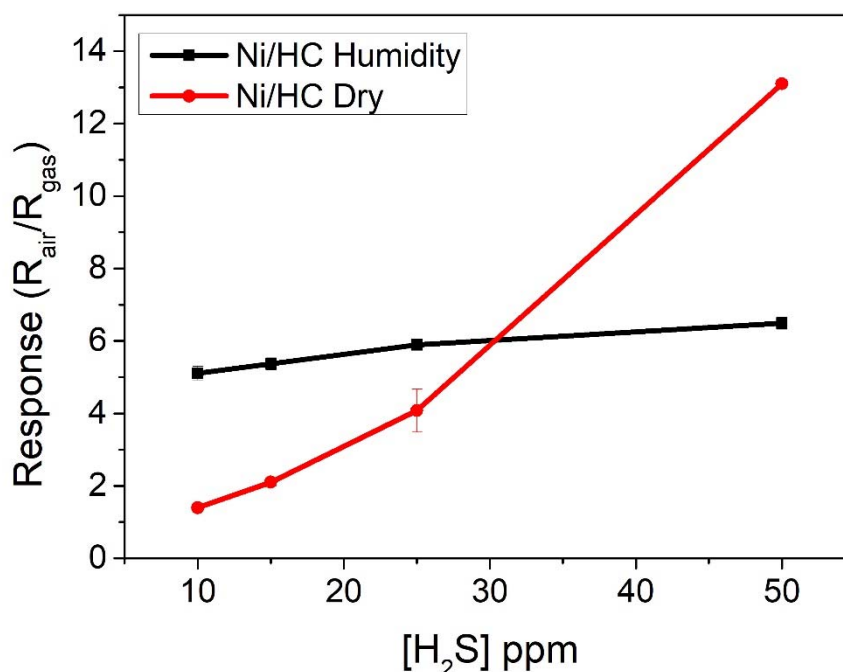
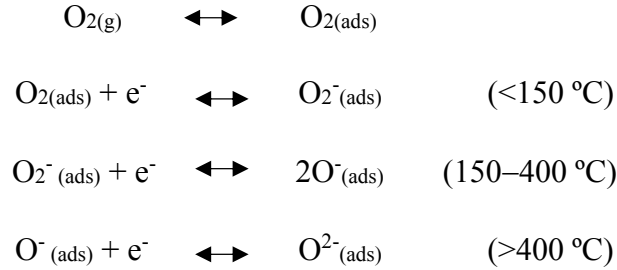


Figure 12. H₂S sensing results comparison between dry and those obtained under 35% of H.R. at 250°C.

It has been reported that in p-type metal oxide nanoparticles supported on n-type metal oxide surfaces, when ambient humidity is present, the host n-type substrate would remain drier due to the higher affinity between the p-type metal oxide (i.e., nickel oxide) and water molecules [35, 36]. At the normal operating temperatures, dissociative adsorption of water molecules takes place resulting in the formation of hydroxyl groups [8] at the surface of nickel oxide nanoparticles and, to a lesser extent, at the surface of tungsten oxide nanowires. The competitive reaction with oxygen surface species of hydrogen sulfide and water molecules could explain the overall decrease in sensitivity caused by the presence of ambient moisture. However, the interaction of hydrogen sulfide with hydroxyl groups and subsequent relaxation of the space charge zone at the p-n interfaces resulting in electronic charge transfer towards the tungsten oxide nanowires could explain the higher responses recorded for low hydrogen sulfide concentrations.

3.5 Hydrogen sulfide detection mechanism

The hydrogen sulfide sensing mechanism in Ni-loaded tungsten oxide nanowires is temperature dependent, as the oxygen species adsorbed on the surface of the nickel oxide differ with temperature [37]:



Based on the results observed, one reaction that governs the process of the detection of H₂S consists of an oxidation process that consumes adsorbed surface species and results in the generation of free electronic charge. This process is as follows:

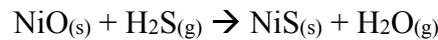


which holds when the operating temperature is 150 °C and oxygen surface species consist basically of adsorbed molecular oxygen. Alternatively,

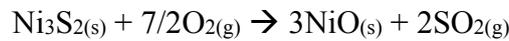
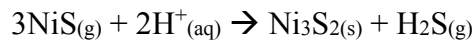


which holds when the operating temperature is 200 °C or 250 °C .

Additionally, another sensing mechanism derived from an electronic sensitization effect caused by the presence of p-type NiO nanoparticles has to be taken into account as well. This mechanism consists in the sulfurization of NiO into Ni_xS_x when the surface of the Ni-loaded tungsten oxide nanowire film is exposed to hydrogen sulfide:



As a result of this sulfurization process, the p-n heterojunctions are destroyed and the overall electrical conductivity of the gas-sensitive film is increased. Even though, a recovery process is also proposed to regenerate the nickel oxide nanoparticles when hydrogen sulfide is removed from the sensor environment [38]:



However, this recovery may be only partial as XPS analysis confirms the presence of Ni_xS_x and $\text{Ni}_x\text{S}_x\text{O}_x$ species on the surface of used sensors. Further details can be found in the Supporting Information.

4. Conclusions

An AACVD process has been employed to grow Ni loaded tungsten oxide nanowires employing tungsten hexacarbonyl and Ni(II) acetylacetonate as precursors. A two-step strategy is needed in which pure tungsten oxide nanowires are grown at first and, these are loaded with Ni-containing nanoparticles in the second step. This ensures that wide range of metal loading can be achieved with high effectivity. HR-TEM analysis has shown that tungsten oxide nanowires are single crystalline and that Ni-containing nanoparticles are about 2 nm in diameter. In general Ni nanoparticles are homogeneously distributed over the tungsten oxide nanowire surface. At high Ni loadings, nanoparticles keep their size unchanged, however they show a tendency to form agglomerates, especially at the tips of tungsten nanowires. XPS analysis has revealed that nanoparticles consist of nickel oxides.

The gas sensing properties of the different nanomaterials grown have been studied. The loading of tungsten oxide with nickel oxide nanoparticles has a positive effect for increasing the sensitivity and selectivity of the resulting nanomaterial to hydrogen sulfide. A five-fold increase in the response towards hydrogen sulfide has been measured. This improvement can be attributed to a chemical sensitization effect in which the nickel oxide nanoparticles increase the amount of adsorbed, reactive surface species, combined to an electronic sensitization effect in which p-type nickel oxide nanoparticles become metallic Ni_xS_x upon exposure to hydrogen sulfide. Furthermore, Ni-loaded tungsten oxide nanowire sensors show enough responsiveness in the units of ppm range of hydrogen sulfide concentrations, even in the presence of humidity. Therefore, this nanomaterial shows good potential for the development of resistive sensors able to monitor the presence of hydrogen sulfide in the ambient, under real application conditions.

Acknowledgements

This work was funded in part by MINECO and FEDER via grant no. TEC2015-71663-R, by AGAUR under grant. 2017SGR 418 and by FNRS via PLAFON and FITTED projects. E.N. gratefully acknowledges a doctoral fellowship from MINECO grant no. BES-2016-076582. E.L. is supported by the Catalan institution for Research and Advanced Studies via the 2012 Edition of the ICREA Academia Award. C.B. is a research Associate of the FNRS (Belgium).

References

1. Akimoto, H. (2003). Global Air Quality and Pollution. *Science*, 302(5651), 1716-1719. doi:10.1126/science.1092666
2. Kampa, M., & Castanas, E. (2008). Human health effects of air pollution. *Environmental Pollution*, 151(2), 362-367. doi:10.1016/j.envpol.2007.06.012
3. Fine, G. F., Cavanagh, L. M., Afonja, A., & Binions, R. (2010). Metal Oxide Semiconductor Gas Sensors in Environmental Monitoring. *Sensors*, 10(6), 5469-5502. doi:10.3390/s100605469
4. Kanan, Sofian M., El-Kadri, Oussama M., Abu-Yousef, Imad A. and Kanan, Marsha C. (2009). Semiconducting Metal Oxide Based Sensors for Selective Gas Pollutant Detection. *Sensors*, 9(10), 8158–8196. doi:10.3390/s91008158.
5. Yamazoe, N., Sakai, G., & Shimanoe, K. (2003). Oxide Semiconductor Gas Sensors. *Catalysis Surveys from Asia*, 7(1), 63-75. doi:10.1023/A:1023436725457
6. Galatsis, K., Cukrov, L., Wlodarski, W., McCormick, P., Kalantar-Zadeh, K., Comini, E., & Sberveglieri, G. (2003). p- and n-type Fe-doped SnO₂ Gas Sensors Fabricated by the Mechanochemical Processing Technique. *Sensors and Actuators B: Chemical*, 93(1-3), 562-565. doi:10.1016/s0925-4005(03)00233-8
7. Kanazawa, E., Sakai, G., Shimanoe, K., Kanmura, Y., Teraoka, Y., Miura, N., & Yamazoe, N. (2001). Metal oxide semiconductor N₂O sensor for medical use. *Sensors and Actuators B: Chemical*, 77(1-2), 72-77. doi:10.1016/s0925-4005(01)00675-x
8. S. Roso, C. Bittencourt, P. Umek, O. González, F. Güell, A. Urakawa, E. Llobet (2016): Synthesis of single Crystalline In₂O₃ Octahedra for the Selective Detection of NO₂ and H₂ at trace levels. *J. Mater. Chem. C*, **4**, 9418.
9. Newrefl Hübner, M., Simion, C., Tomescu-Stănoiu, A., Pokhrel, S., Bârsan, N., & Weimar, U. (2011). Influence of humidity on CO sensing with p-type CuO thick film gas sensors. *Sensors and Actuators B: Chemical*, 153(2), 347-353. doi:10.1016/j.snb.2010.10.046
10. Matsushima, S., Teraoka, Y., Miura, N., & Yamazoe, N. (1988). Electronic Interaction between Metal Additives and Tin Dioxide in Tin Dioxide-Based Gas Sensors. *Japanese Journal of Applied Physics*, 27(Part 1, No. 10), 1798-1802. doi:10.1143/jjap.27.1798

11. Conner, W. C., & Falconer, J. L. (1995). Spillover in Heterogeneous Catalysis. *Chemical Reviews*, 95(3), 759-788. doi:10.1021/cr00035a014
12. Kamble, V. B., & Umarji, A. M. (2015). Effect of Pt doping on the gas sensing properties of porous chromium oxide films through a kinetic response analysis approach. *RSC Advances*, 5(35), 27509-27516. doi:10.1039/c5ra02186c
13. Wang, C., Yin, L., Zhang, L., Xiang, D. and Gao, R. (2010). Metal Oxide Gas Sensors: Sensitivity and Influencing Factors. *Sensors*, 10(3), 2088–2106. doi:10.3390/s100302088.
14. Annanouch, Fatima E., Haddi, Z., Vallejos, S., Umek, P. Guttman, P., Bittencourt, C. and Llobet, E. (2015). Aerosol-Assisted CVD-Grown WO₃ Nanoneedles Decorated with Copper Oxide Nanoparticles for the Selective and Humidity-Resilient Detection of H₂S. *ACS Applied Materials & Interfaces*, 7(12), 6842–6851. doi:10.1021/acsami.5b00411.
15. Annanouch, Fatima E., Haddi, Z., Ling, M., Di Maggio, F., Vallejos, S., Vilic, T., Y. Zhu, Y., Shujah, T., Umek, P., Bittencourt, C., Blackman, C. and Llobet, E. (2016). Aerosol-Assisted CVD-Grown PdO Nanoparticle-Decorated Tungsten Oxide Nanoneedles Extremely Sensitive and Selective to Hydrogen. *ACS Applied Materials & Interfaces*, 8(16), 10413–10421. doi:10.1021/acsami.6b00773.
16. Vallejos, S., Umek, P., Stoycheva, T., Annanouch, F., Llobet, E., Correig, X. de Marco, P., Bittencourt, C. and Blackman, C. (2013). Single-Step Deposition of Au- and Pt-Nanoparticle-Functionalized Tungsten Oxide Nanoneedles Synthesized Via Aerosol-Assisted CVD, and Used for Fabrication of Selective Gas Microsensor Arrays. *Advanced Functional Materials*, 23(10), 1313–1322. doi:10.1002/adfm.201201871.
17. Sato, H., Minami, T., Takata, S., & Yamada, T. (1993). Transparent conducting p-type NiO thin films prepared by magnetron sputtering. *Thin Solid Films*, 236(1-2), 27-31. doi:10.1016/0040-6090(93)90636-4
18. Lany, S., Osorio-Guillén, J., & Zunger, A. (2007). Origins of the doping asymmetry in oxides: Hole doping in NiO versus electron doping in ZnO. *Physical Review B*, 75(24). doi:10.1103/physrevb.75.241203
19. Kim, H., Choi, K., Kim, K., Na, C. W., & Lee, J. (2012). Highly sensitive C₂H₅OH sensors using Fe-doped NiO hollow spheres. *Sensors and Actuators B: Chemical*, 171-172, 1029-1037. doi:10.1016/j.snb.2012.06.029
20. Yoon, J., Kim, H., Kim, I., & Lee, J. (2013). Electronic sensitization of the response to C₂H₅OH of p-type NiO nanofibers by Fe doping. *Nanotechnology*, 24(44), 444005. doi:10.1088/0957-4484/24/44/444005
21. Cho, N. G., Woo, H., Lee, J., & Kim, I. (2011). Thin-walled NiO tubes functionalized with catalytic Pt for highly selective C₂H₅OH sensors using electrospun fibers as a sacrificial template. *Chemical Communications*, 47(40), 11300. doi:10.1039/c1cc13876f
22. Yu, T., Cheng, X., Zhang, X., Sui, L., Xu, Y., Gao, S., Huo, L. (2015). Highly sensitive H₂S detection sensors at low temperature based on hierarchically structured NiO porous nanowall arrays. *Journal of Materials Chemistry A*, 3(22), 11991-11999. doi:10.1039/c5ta00811e

23. Wang, Z., Nayak, P. K., Caraveo-Frescas, J. A., & Alshareef, H. N. (2016). Recent Developments in p-Type Oxide Semiconductor Materials and Devices. *Advanced Materials*, 28(20), 3831-3892. doi:10.1002/adma.201503080
24. Wang, J., Yang, P., & Wei, X. (2015). High-Performance, Room-Temperature, and No-Humidity-Impact Ammonia Sensor Based on Heterogeneous Nickel Oxide and Zinc Oxide Nanocrystals. *ACS Applied Materials & Interfaces*, 7(6), 3816-3824. doi:10.1021/am508807a
25. Fomekong, R. L., Lahem, D., Debliquy, M., Yunus, S., Ngolui, J. L., & Delcorte, A. (2016). Ni 0.9 Zn 0.1 O/ZnO nanocomposite prepared by malonate coprecipitation route for gas sensing. *Sensors and Actuators B: Chemical*, 231, 520-528. doi:10.1016/j.snb.2016.03.099
26. Sun, C., & Dutta, P. K. (2016). Selective detection of part per billion concentrations of ammonia using a p-n semiconducting oxide heterostructure. *Sensors and Actuators B: Chemical*, 226, 156-169. doi:10.1016/j.snb.2015.11.085
27. Li, W., Zhang, X., & Guo, X. (2017). Electrospun Ni-doped SnO₂ nanofiber array for selective sensing of NO₂. *Sensors and Actuators B: Chemical*, 244, 509-521. doi:10.1016/j.snb.2017.01.022
28. Noh, W., Shin, Y., Kim, J., Lee, W., Hong, K., Akbar, S. A., & Park, J. (2002). Effects of NiO addition in WO₃-based gas sensors prepared by thick film process. *Solid State Ionics*, 152-153, 827-832. doi:10.1016/s0167-2738(02)00341-7
29. Vuong, N. M., Trung, T. N., Hien, T. T., Chinh, N. D., Quang, N. D., Lee, D., Kim, D. (2015). Ni₂O₃ Decoration of WO₃ Thin Film for High Sensitivity NH₃ Gas Sensor. *Materials Transactions*, 56 (9), 1354-1357. doi:10.2320/matertrans.ma201572
30. Vilic, T., & Llobet, E. (2016). Nickel Doped WO₃ Nanoneedles Deposited by a Single Step AACVD for Gas Sensing Applications. *Procedia Engineering*, 168, 206-210. doi:10.1016/j.proeng.2016.11.163
31. Xie, F. Y.; Gong, L.; Liu, X.; Tao, Y. T.; Zhang, W. H.; Chen, S. H.; Meng, H.; Chen, J. (2012). XPS Studies on Surface Reduction of Tungsten Oxide Nanowire Film by Ar⁺ Bombardment. *J. Electron Spectrosc. Relat. Phenom.* 185, 112–118.
32. Bittencourt, C., Llobet, E., Ivanov, P., Vilanova, X., Correig, X., Silva, M.A.P., Nunes, L.A.O., Pireaux, J.J. (2004). Ag induced modifications on WO₃ films studied by AFM, Raman and x-ray photoelectron spectroscopy, *Journal of Physics D: Applied Physics*, 37 (24), pp. 3383-3391.
33. Ottaviano, L., Bussolotti, F., Lozzi, L., Passacantando, M., La Rosa, S., Santucci, S. (2003). Core Level and Valence Band Investigation of WO₃ Thin Films with Synchrotron Radiation. *Thin Solids Films*, 436, 9–16.
34. UNITED STATES DEPARTMENT OF LABOR. (n.d.). Retrieved January 21st, 2018, from <https://www.osha.gov/SLTC/hydrogensulfide/standards.html>
35. Lackner, E., Krainer, J., Wimmer-Teubenbacher, R., Sosada, F., Gspan, C., Rohrer, K., Koeck, A. (2016). CMOS Integrated Nanocrystalline SnO₂ Gas Sensors for CO Detection. *Procedia Engineering*, 168, 297-300.

doi:10.1016/j.proeng.2016.11.200

36. Choi, K., Hübner, M., Haensch, A., Kim, H., Weimar, U., Barsan, N., & Lee, J. (2013). Ambivalent effect of Ni loading on gas sensing performance in SnO₂ based gas sensor. *Sensors and Actuators B: Chemical*, 183, 401-410. doi:10.1016/j.snb.2013.04.007
37. Ahire, D. V., Patil, G. E., Kajale, D. D., Gaikwad, V. B., & Jain, G. H. (n.d.). Chapter 10 Nanostructured Nickel Oxide by Hydrothermal Route for Gas Sensing Applications. In *Sensing Technology: Current Status and Future Trends I, Smart Sensors, Measurement and Instrumentation* 7 (pp. 181-193). doi:10.1007/978-3-319-02318-2_10
38. Atimtay, A. T., & Harrison, D. P. (2013). *Desulfurization of Hot Coal Gas*. Berlin: Springer Berlin.